COMPUTER METHODS AND PROGRAMS IN BIOMEDICINE XXX (2014) XXX–XXX

journal homepage: www.intl.elsevierhealth.com/journals/cmpb

A comparative approach of four different image registration techniques for quantitative assessment of coronary artery calcium lesions using intravascular ultrasound

Tadashi Araki[a], *Nobutaka Ikeda*[b], *Nilanjan Dey*[c], *Sayan Chakraborty*[c], *Luca Saba*[d], *Dinesh Kumar*[e], *Elisa Cuadrado Godia*[f], *Xiaoyi Jiang*[g], *Ajay Gupta*[h], *Petia Radeva*[i,j], *John R. Laird*[k], *Andrew Nicolaides*[l,m], *Jasjit S. Suri*[c,e,n,*]

[a] *Division of Cardiovascular Medicine, Toho University Ohashi Medical Center, 2-17-6 Ohashi, Meguro-ku, Tokyo, Japan*
[b] *Division of Cardiovascular Medicine, Centre for Global Health and Medicine (NCGM), 1-21-1 Toyama, Shinjuku-ku, Tokyo, Japan*
[c] *Point of Care Devices, Global Biomedical Technologies, Inc., Roseville, CA, USA*
[d] *Azienda Ospedaliero Universitaria (A.O.U.) di Cagliari – Polo di Monserrato, Università di Cagliari, s.s. 554 Monserrato, Cagliari 09045, Italy*
[e] *Stoke Screening and Monitoring Division, AtheroPoint™ LLC, Roseville, CA, USA*
[f] *IMIM – Hospital del Mar, Passeig Marítim 25-29, Barcelona, Spain*
[g] *Department of Computer Science, University of Münster, Münster, Germany*
[h] *Department of Radiology, Weill Cornell Medical College, New York Presbyterian Hospital, New York, USA*
[i] *MILab, CVC, University of Barcelona, Barcelona, Spain*
[j] *Applied Mathematics and Analysis Department, University of Barcelona, Barcelona, Spain*
[k] *UC Davis Vascular Center, University of California, Davis, CA, USA*
[l] *Vascular Screening and Diagnostic Centre, London, UK*
[m] *Department of Biological Sciences, University of Cyprus, Nicosia, Cyprus*
[n] *Electrical Engineering Department (Affl.), Idaho State University, Pocatello, ID, USA*

ARTICLE INFO

Article history:
Received 30 April 2014
Received in revised form
20 November 2014
Accepted 21 November 2014

Keywords:
IVUS
Motion
Registration

ABSTRACT

In IVUS imaging, constant linear velocity and a constant angular velocity of 1800 rev/min causes displacement of the calcium in subsequent image frames. To overcome this error in intravascular ultrasound video, IVUS image frames must be registered prior to the lesion quantification. This paper presents a comprehensive comparison of four registration methods, namely: Rigid, Affine, B-Splines and Demons on five set of calcium lesion quantification parameters namely: (i) the mean lesion area, (ii) mean lesion arc, (iii) mean lesion span, (iv) mean lesion length, and (v) mean lesion distance from catheter.

Using our IRB approved data of 100 patient volumes, our results shows that all four registrations showed a decrease in five calcium lesion parameters as follows: for Rigid registration, the values were: 4.92%, 5.84%, 5.89%, 5.27%, and 4.57%, respectively, for Affine

* *Corresponding author at*: Stoke Screening and Monitoring Division, AtheroPoint™ LLC, Roseville, CA, USA.
E-mail address: jasjit.suri@atheropoint.com (J.S. Suri).

http://dx.doi.org/10.1016/j.cmpb.2014.11.006
0169-2607/Published by Elsevier Ireland Ltd.

Rigid
Demons
AtheroEdge™

registration the values were: 6.06%, 6.51%, 7.28%, 6.50%, and 5.94%, respectively, for B-Splines registration the values were: 7.35%, 8.03%, 9.54%, 8.18%, and 7.62%, respectively, and for Demons registration the five parameters were 7.32%, 8.02%, 10.11%, 7.94%, and 8.92% respectively.

The relative overlap of identified lesions decreased by 5.91% in case of Rigid registration, 6.23% in case of Affine registration, 4.48% for Demons registration, whereas it increased by 3.05% in case of B-Splines registration. Rigid and Affine transformation-based registration took only 0.1936 and 0.2893 s per frame, respectively. Demons and B-Splines framework took only 0.5705 and 0.9405 s per frame, respectively, which were significantly slower than Rigid and Affine transformation based image registration.

Published by Elsevier Ireland Ltd.

1. Introduction

Plaque deposition in coronary arteries leads to coronary artery disease, which is a large component of the broad disease process known as atherosclerosis. During the atherosclerosis disease formation, soft plaque is formed turning to calcium at later stage of the disease [1]. The calcium measurement and location provides information which can help during the interventional procedures [2,3].

During the IVUS imaging procedure, the catheter pullback maintaining a linear constant velocity and a constant angular velocity of 1800 rev/min causes the calcium to get displaced laterally, longitudinal and/or rotational fashion [4]. Cardiac pulsatility along with motion related to catheter pullback can cause faulty measurements of calcium lesions in subsequent frames. To reduce these errors, IVUS image registration is required.

Though, the accurate registration of medical images is an active research field, the amount of work done in the field of IVUS image registration is relatively small. Strain measurement in coronary arteries using IVUS and deformable images was proposed by Veress et al. [7]. The main focus of this study was to calculate the efficacy of an image registration technique warping. From paired IVUS images, warping helped to determine the strains in plaques and coronary arteries. Multimodal registration of IVUS images and angiography was proposed by Rotger et al. [8]. The objective of this work was to develop a technique which would fuse information from angiograms and IVUS images by utilizing a point of the vessel in the angiograms and its corresponding IVUS image. Katouzian et al. [9] proposed a framework that was capable of tissue labelling and then registering against histology [10]. The correspondence was achieved by making a 3-D reconstruction of the IVUS catheter's path from its projection in the angiography [12]. Non-rigid registration of vessel structures in IVUS images [11] was introduced by Amores and Radeva [13]. An algorithm applicable to grey level medical images of non-rigid bodies such as coronary vessels was proposed in this work. With the help of IVUS image registration [14] managed to quantify the cross-sectional artery wall motion. In this work, a robust method was reported to track cross-sectional displacements of an artery wall using two different intravascular ultrasound (IVUS) images acquired at two different pressure levels respectively. The report defines the correspondence by creating a 3-D reconstruction of the IVUS catheter's path from its projection in the angiographic data and using this information to set the IVUS planes.

A fast rigid registration of vascular structures in IVUS sequences was proposed by Gatta et al. [15]. In this work, an algorithm was proposed which not only reduced the saw-shaped oscillation, but also aligned the vascular structures successfully. An automatic approach of vessel lumen segmentation was proposed by Balocco et al. [16]. This automated system used grow cut algorithm to extract the combined model-based temporal information from successive frames of the sequence. With the help of iconic and geometric features, Gupta et al. [17] introduced a new registration system for carotid ultrasound images. A novel hybrid registration technique was proposed in this study which closed the difference between the feature-based image registration techniques as well as the intensity-based registration techniques. Analysis of this work was done with the help of image registration. Non-rigid image registration metric using self-similarity weighted mutual information was proposed by Rivaz et al. [18]. In this work, a self-similarity weighted graph-based implementation of α mutual information (α-MI) for non-rigid image registration was introduced. Image-based co-registration of angiography and IVUS was reported by Wang et al. [19]. This work presented a new hybrid technique which was able to solve the problem created during the registration of 2-D angiography and IVUS. Bidirectional elastic image registration using B-Splines Affine transformation was proposed by Gu et al. [20]. In this work, a registration scheme was proposed which was termed as B-Splines Affine transformation (BSAT). It was capable of elastically aligning two images.

To the best of our knowledge, no previous work has analyzed the size and shape change of calcium lesion after applying an IVUS image registration paradigm. Similarly, to our knowledge no previous study has compared the quantification of lesion changes using four types of IVUS image registration methods. In this work, we studied the effect of registration using Rigid (which involves rotations and translations) and Affine transformation [21], and compared them to local transformation based non-rigid registration techniques using B-Splines and non-parametric Demons registration.

Our purpose was to analyze changes in calcium quantification parameters and study the effect of four different registration techniques: Rigid transformation based, Affine transformation based, B-Splines-based non-rigid free form

Please cite this article in press as: T. Araki, et al., A comparative approach of four different image registration techniques for quantitative assessment of coronary artery calcium lesions using intravascular ultrasound, Comput. Methods Programs Biomed. (2014), http://dx.doi.org/10.1016/j.cmpb.2014.11.006

deformation (FFD) and Demons algorithm based registration. The calcium parameters we searched for, in shape-based feature analysis of coronary calcium and its quantification in consecutive frames [5,6] include the following: (i) mean centreline lesion length, (ii) lesion distance to catheter centre, (iii) mean span (arc angle) of the detected lesion, (iv) mean lesion subtended angle, (v) lesion area, and (vi) mean normalized volume.

We aimed to assess accuracy and precision measurement of calcium detection and volume computation as an effect of these different registration methods. Our study also evaluated the performance of our four registration methods using different similarity and overlap metrics. In addition, the registration effect on the polar representation of calcium layout in the IVUS temporal layout is shown. The purpose of polar representation was mainly for understanding the global representation of calcium layout for a particular ethnic group. Lastly, we have also studied the time needed for image registration using the four IVUS registration techniques.

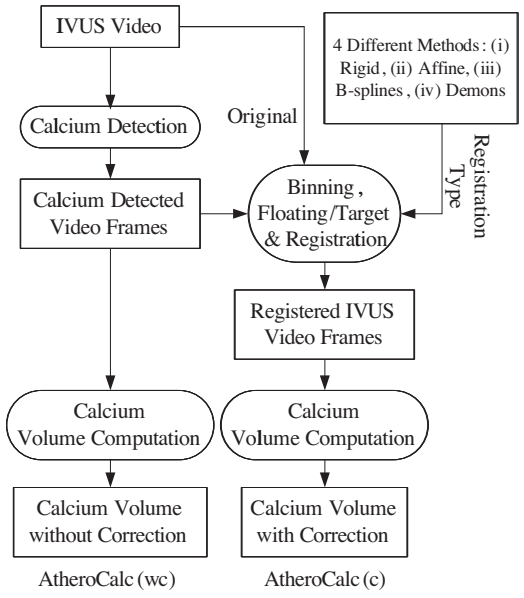

Fig. 1 – Block diagram of the proposed system registration in calcium detected frames.

2. Materials and methods

2.1. *Demographics*

A single-centre study was conducted on 146 patients who were selected from consecutive 160 stable angina pectoris (SAP) patients. Between July 2009 and December 2010 these patients were subjected to percutaneous coronary intervention (PCI), iMap-IVUS, and carotid ultrasound examination. When angina remained unchanged for more than 2 months or a stress test resulted positive, SAP was defined of class I or II. The target lesion was de-novo (>75% angiographic stenosis by visual estimation). A combination of left ventricular wall motion abnormalities, ECG findings, angiographic lesion morphology, and scintigraphic defects identified the target lesion. The patients were pre-medicated with a combination dose of Clopidogrel (75 mg/day) with Aspirin (100 mg/day) before the PCI procedure. To achieve activated partial thromboplastin time of less than 250 s, the patients were given an intravenous unfractionated heparin before the procedure. The drug glycoprotein IIb/IIIa inhibitor is not approved in Japan and therefore this drug was not administered to any of the patients. A balloon was inserted in the arteries of patients suffering from severe stenosis. This procedure was done prior to IVUS examinations to dilate their arteries. We selected 100 patients randomly from pool of 146 patients for our current study.

2.2. *IVUS image acquisition*

In this study, there was an intra-coronary administration of 125–250 mg of nitroglycerin, which was performed on every patient. This procedure was followed by stenting. For IVUS data acquisition, a 40 MHz IVUS catheter (Atlantis SR Pro, Boston Scientific) was used. The imaging of the target lesion was done when the catheter, which had advanced beyond the lesion, experienced automatic pullback at a speed of 0.5 mm/s. This acquired data was stored on a hard disc for off-line analysis. Very high intensity echo reflectors which engaged a vessel circumference of more than 90° and length more than 1 mm, show the ultrasound signal attenuation in an atherosclerotic plaque. These high intensity echo reflectors also demonstrate the presence of echo signal attenuation on IVUS. IVUS data was digitally recorded in a DICOM file (.dcm) format. For analysis and convenience for our study, we converted and tested the data on QuickTime (.mov) file extension.

2.3. *Binning strategy for preparation of IVUS image registration*

We solve the problem created by spatio-temporal localization changes of lesion, by increasing correlation between two consecutive frames using the frame registration process. Sensitivity of the registration process increases as the distance between moving and target frames decreases. However, the erroneous selection of target frames can lead to meaningless registration. To resolve this problem, in our study, a bin selection strategy was introduced in which we divided the entire video into a bin size of 10. In case of multiple calcium hits in any bin, that bin was further partitioned into two halves ($k = 5$). The middle frame or the frame common in both halves was considered as the target frame. We repeated this process until all bins were processed. Fig. 1 illustrates the binning strategy and its usage in the registration process. Controlling the temporal frame selection to have a meaningful correction in calcium volumes along with retaining validation and benchmarking infrastructure is the main objective of this strategy.

2.4. *Automated calcium detection in IVUS video*

The calcium detection algorithm uses a suppression mechanism as discussed in previous patented research [5,6] (called AtheroCalc system). It proposes a system which suppresses the adventitia [22] by creating an adventitial mask thereby

Please cite this article in press as: T. Araki, et al., A comparative approach of four different image registration techniques for quantitative assessment of coronary artery calcium lesions using intravascular ultrasound, Comput. Methods Programs Biomed. (2014), http://dx.doi.org/10.1016/j.cmpb.2014.11.006

allowing the remaining calcium lesion to be extracted from the non-suppressed region. IVUS videos collected for our study were recorded in QuickTime (.mov) format which is a lossy compression method and results in lower quality compared to the original DICOM, which may result in under-estimation of actual calcium region and volume in IVUS images. To overcome this issue, gamma transformation was used in our study, which intensifies gradient changes leading to stretching the contrast. Gamma value refers to the value which remained constant in our study, for each and every video frame. It has been observed that maximum gradient changes occur in the media-adventitia [5,6] border area. Applying the median filter, individual pixels with extreme values were removed from the images, which causes image blurring. Median filter also leads to adventitia mask generation, although, the calcium region is not affected by the median filter. Otsu's local statistical threshold was used to binarize the generated image, which minimizes intra-class variance. It was assumed that the video frame has a two-class paradigm: adventitia region and its background. Otsu's method resulted in a higher threshold [23] as the adventitia region edge was a brighter edge away from the background. Connected component analysis (CCA) was used in order to remove scattered binary lumen regions. For gaining the maximum binary adventitia and removal of islands CCA was employed. The adventitia was used as a mask which suppressed the extracted adventitia, which helped to generate the grayscale image with calcium. The only bright region of calcium was extracted by further iterating one more step of Otsu's local statistical threshold. The calcium region was segmented while the white dotted markers in IVUS frames are retained. The calcium region present in the coronary wall [5,6] was selected based on size of the object to filter the calcium region. This study is more geared towards the comprehensive comparison of image registration and its effect on image segmentation. For more details on image segmentation, we suggest readers to see the previous works done by Araki et al. [5,6]. In the next few sections we will discuss in detail on the registration methods.

2.5. Four image registration methods

The purpose of IVUS image registration is to overcome the problem of inaccurate lesion quantification due to inherent limitations of IVUS imaging, i.e., motion of catheter as it is withdrawn. The consecutive frames may not be aligned due to rotation/twisting of catheter resulting in same lesion appearing at different locations in these frames. There might also be non-rigid deformation due to soft geometry of the vessel walls. In addition, the consecutive frames may not be parallel to each other. In this paper, we primarily focus on reducing lesion measurement inaccuracies caused by moving of catheter in-plane. We study four registration techniques that incrementally model deformation: Rigid, Affine, B-Splines and Demons.

2.5.1. Rigid registration

Rigid transformation involves rotation, translation and/or their combination. The Rigid transformation preserves the distance between two points and angles made by the points of the model. Rigid transformation represents the simplest of transformations studied in this paper, with least number of parameters: x- and y-translation and a rotation angle.

2.5.2. Affine registration

Affine transformation involves reflection and shear mapping along with mentioned parameters of Rigid transformation. Affine transformation can model global stretching and skewing more accurately than Rigid transformation and hence, may be more tolerant of small angles between consecutive planes. We use a least square based approach [2] to minimize the biased error between reference and target frames.

2.5.3. B-Splines

Rigid and Affine transformations are global transformations and do not recover any local deformation. B-Splines registration provides one suitable alternative to perform deformable image registration (DIR). B-Splines are locally supported and provide a continuous transformation over entire image and have highly desirable properties as basis functions to model real-world problems. Salient-feature-based registration (SFBR), free-form deformation (FFD) using cubic B-Splines and non-parametric registration technique based on diffeomorphic Demons are well known methods of DIR in medical image analysis.

In SFBR, the term "salient features" refers to the prominent and distinct features present in medical images. As earlier discussed, to show or detect atherosclerotic plaque, IVUS technique is used in imaging coronary [24] artery. The plaque consists of soft plaque and hard plaque like calcium. Clearly, in most cases, due to the image quality or due to the nature of image acquisition there are local geometric differences in the detected calcium which can lead to a significant number of missing anchor points. As a result, failure is discovered in feature-based technique like SFBR.

B-Splines FFD algorithm [25] is used in order to maximize the similarity measure while deforming an image and modifying the mesh of control points, which only affects the neighbouring points. A mesh is generated by these control points. B-Splines interpolation results in dense transformation fields between control points. The deformation in B-Splines is free-form deformation (FFD) based on B-Splines which is a powerful tool for modelling 3D deformations.

Our system used uniform cubic B-Splines in order to apply transformation on IVUS frames. The following equations [3] were used to generate a curve:

$$X(v) = z_3 v^3 + z_2 v^2 + z_1 v^1 + z_0, \quad (1)$$

where, 1, z_0, z_1, z_2 and z_3 refers to the parameters used.

For each and every curve segment, the value of v varies between 0 and 1. The cubic functions which are used for each segment has an impact on uniform cubic B-Splines [18] curves. Following are the three continuity requirements for each segment:

1. *Positional continuity*: If two segments b and b+1, who are positioned next to each other having same ending and starting point, we concluded that the segments involved are in positional continuity.

Please cite this article in press as: T. Araki, et al., A comparative approach of four different image registration techniques for quantitative assessment of coronary artery calcium lesions using intravascular ultrasound, Comput. Methods Programs Biomed. (2014), http://dx.doi.org/10.1016/j.cmpb.2014.11.006

2. *Tangential continuity*: If two segments b and b+1 have no abrupt changes in slope as a result of transition, the segments are in tangential continuity.
3. *Curvature continuity*: Curvature continuity refers to zero polarity change in slope during transition between two consecutive segments b and b+1.

Each segment in the curves must follow these continuity requirements. Control points are those points that play a vital role to shape of the curve. Each control point must have few weighting functions. Selecting the weights and using the continuity requirements, the following weighting [3] basis functions can be derived for four control points:

$$\left.\begin{aligned}\alpha_0(v) &= \frac{1}{6}v^3\\ \alpha_1(v) &= \frac{1}{6}[1+3v+3v^2-3v^3]\\ \alpha_2(v) &= \frac{1}{6}[4-6v^2+3v^3]\\ \alpha_3(v) &= \frac{1}{6}[1-3v+3v^2-3v^3]\end{aligned}\right\} \quad (2)$$

The weighting functions $\alpha_0(v)$, $\alpha_1(v)$, $\alpha_2(v)$ and $\alpha_3(v)$ refers to the weight assigned to the control points. The weighting functions are dependent mainly on the value of v which varies between 0 and 1. The main culprits behind the image transformation are the grid of these B-Splines control points [27] that controls the transformation. For each curve in B-Splines, knot refers to the position where the control points meet. Knots are controlled by Knot vectors (which varies from 0 to 1). In our study, grid spacing and knot vectors were measured according to the image size and the positions of the grid points. The B-Splines coefficients located at the control points also help B-Splines registration. The main challenge of B-Splines registration is to find the right set of parameters.

2.5.4. *Demons*

Thirion's Demons algorithm [28] is a fast non-rigid registration method that can model local deformation. Demons algorithm uses a classical optimization scheme to solve a deformable image registration. The displacement of deviator D' between the target image (t) and the reference image (r) is computed by using the iterative formula as given in Eq. (3).

$$D'^{n}_{i,j} = D'^{n-1}_{i,j} - \frac{(t^{n-1}_{i,j} - r^{0}_{i,j})\nabla r^{0}_{i,j}}{|\nabla r^{0}_{i,j}|^2 + |(t^{n-1}_{i,j} - r^{0}_{i,j})|^2} \quad (3)$$

for $i, j = 1,2,3,\ldots,N$. This iterative equation is subject to the following initial condition:

$$\left.\begin{aligned}D'^{0}_{i,j} &= 0\\ t^{0}_{i,j} &= \widehat{t_{i,j}}\\ r^{0}_{i,j} &= \widehat{r_{i,j}}\end{aligned}\right\} \quad (4)$$

where $\widehat{t_{i,j}}$ and $\widehat{r_{i,j}}$ are intensities of the original static and moving images at the corresponding pixel and N is any positive integer. The methodology of calcium detected frame registration (along with volume computation) using all four registration techniques, Rigid, Affine, B-Splines and Demons algorithm is illustrated in Fig. 1. Details about calcium volume computation are discussed in Section 3.3.

3. Results

3.1. *Comparison of visual representation: Rigid, Affine, B-Splines and Demons*

For automated registration processes, we used MATLAB 2012a (The MathWorks, Natick, MA, USA). Using the protocol discussed in Fig. 1, we ran the registration methods using four techniques: Rigid, Affine, B-Splines, and Demons. Figs. 2 and 3 demonstrate the effect of Rigid, Affine B-Splines and Demons registration on candidate frames side-by-side. The current study was done on a total of 100 patient volumes.

The effect of Rigid, Affine, B-Splines, and Demons registration of the grayscale calcium region and its corresponding 100 strongest feature points is illustrated in Fig. 4. The matched points among those 100 strongest feature points are shown in Fig. 5. Same study was done for specific regions of interest and the results are shown in Fig. 6. Despite a scale change or in-plane rotation, point correspondences between the reference and the target image were found out using point feature matching technique. From Figs. 4–6 it is clear that the numbers of strongest feature points are same in corresponding frames prior to the registration. The change of Cartesian position of those points clearly indicates the spatio-temporal localization changes of the calcium lesion. The technique is also robust to small amount of out-of-plane rotation.

3.2. *Calcium detection and volume computation: before and after registration*

Using the method discussed in Section 2.3 (Automated calcium detection in IVUS video), we segmented calcium regions successfully. In this work, we found the following lesion quantitative parameters (before and after registration): (i) mean centreline lesion length, (ii) lesion distance to catheter centre, (iii) mean span (arc angle) of the detected lesion, (iv) mean lesion subtended angle, (v) lesion area, and (vi) mean normalized volume using integration method (IM) [5,6] computed for four types of registration methods. In the integration method the area per frame of the calcium region was computed by summing all the pixels of the calcium lesion (Fig. 7).

3.3. *Quantification of calcium volume lesions before and after image registration*

Summing the areas in all the calcium detected frames provides the total normalized calcium volume. Fig. 4 illustrates some of our automated lesion quantifying parameters. Lesion quantification parameters' effect is shown in Table 1. Table 1 shows an overestimation of all lesion quantification parameters without registration. The normalized volume change as an effect of Rigid, Affine, B-Splines, and Demons is shown in Fig. 8.

Please cite this article in press as: T. Araki, et al., A comparative approach of four different image registration techniques for quantitative assessment of coronary artery calcium lesions using intravascular ultrasound, Comput. Methods Programs Biomed. (2014), http://dx.doi.org/10.1016/j.cmpb.2014.11.006

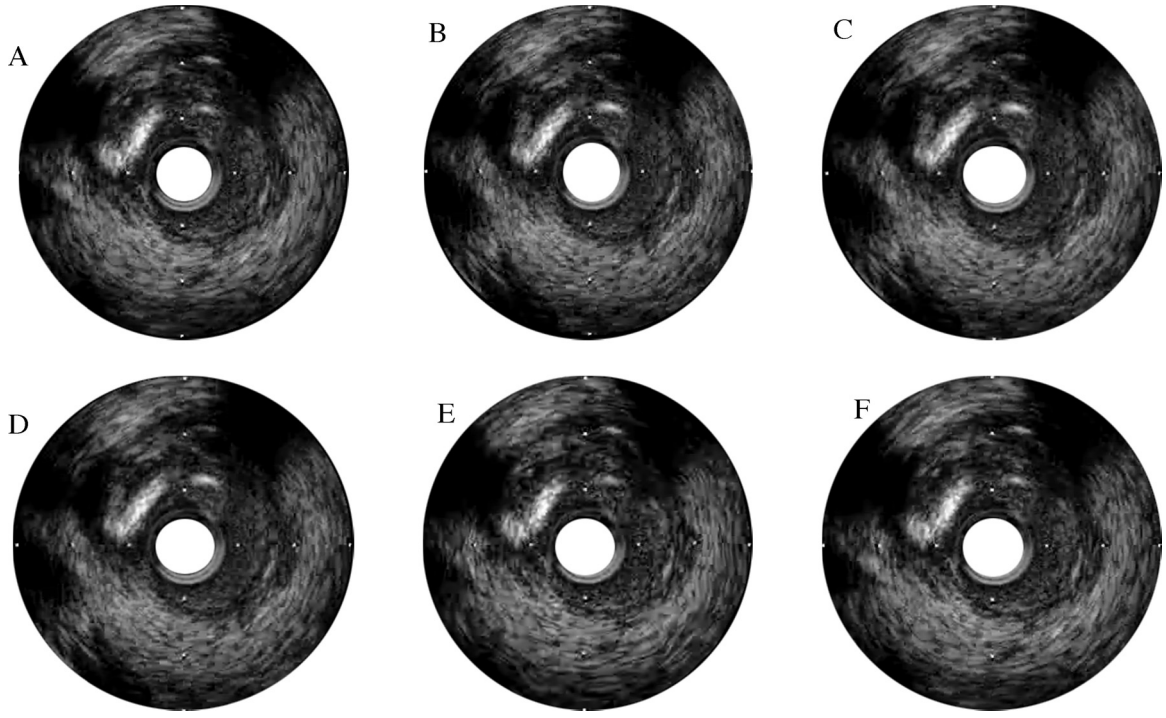

Fig. 2 – IVUS registration: (A) reference frame, (B) target frame, (C) registered target using Rigid, (D) registered target using Affine, (E) registered target using B-Splines, and (F) registered target using Demons.

3.4. *Polar Representation of detected calcium before and after registration*

The polar representation of calcium lesion is a global representation and layout of the calcium lesions. Each dot in the polar representation shows a single patient and represents the centre of calcium. Thus such cluster of dots helps to know the distribution of the lesion built-up for that cohort or particular group of demographics. Fig. 9 shows a presentation of such a cohort using the four different registration techniques.

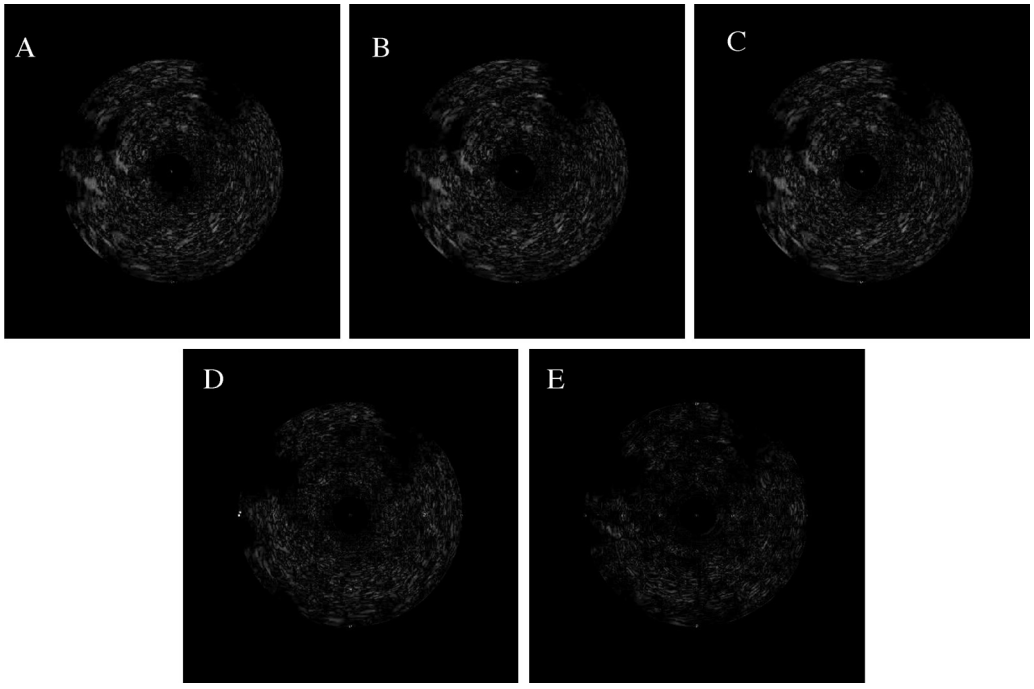

Fig. 3 – Absolute error image (A) before registration, (B) after Rigid registration, (C) after Affine registration, (D) after B-Splines registration, and (E) after Demons registration.

Please cite this article in press as: T. Araki, et al., A comparative approach of four different image registration techniques for quantitative assessment of coronary artery calcium lesions using intravascular ultrasound, Comput. Methods Programs Biomed. (2014), http://dx.doi.org/10.1016/j.cmpb.2014.11.006

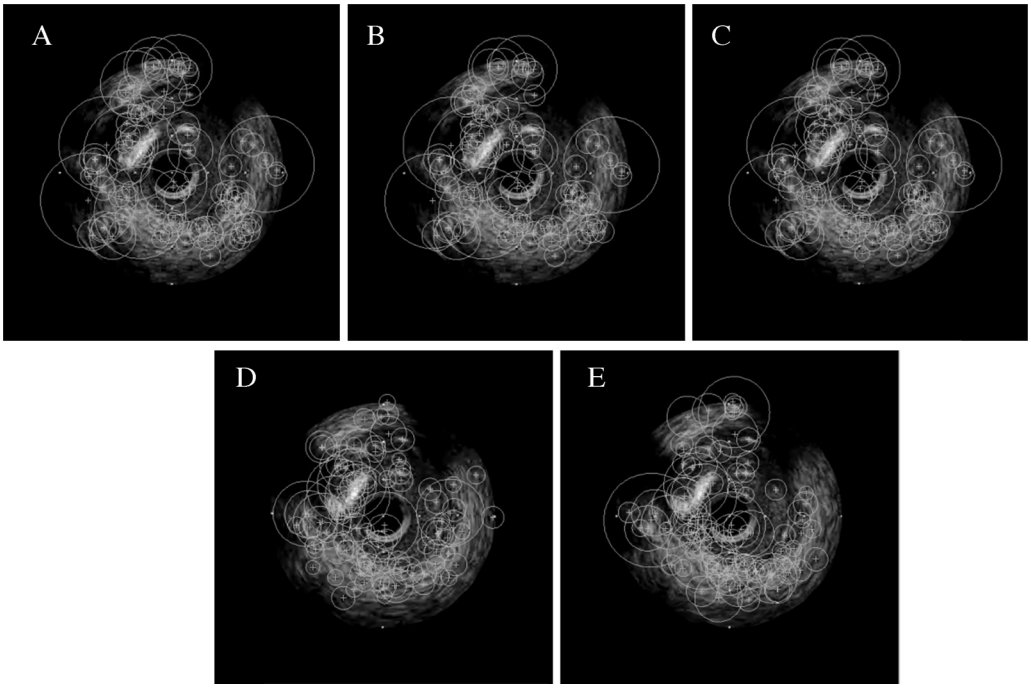

Fig. 4 – 100 strongest feature points: (A) before registration, (B) after Rigid registration, (C) after Affine registration, (D) after B-Splines registration, and (E) after Demons registration.

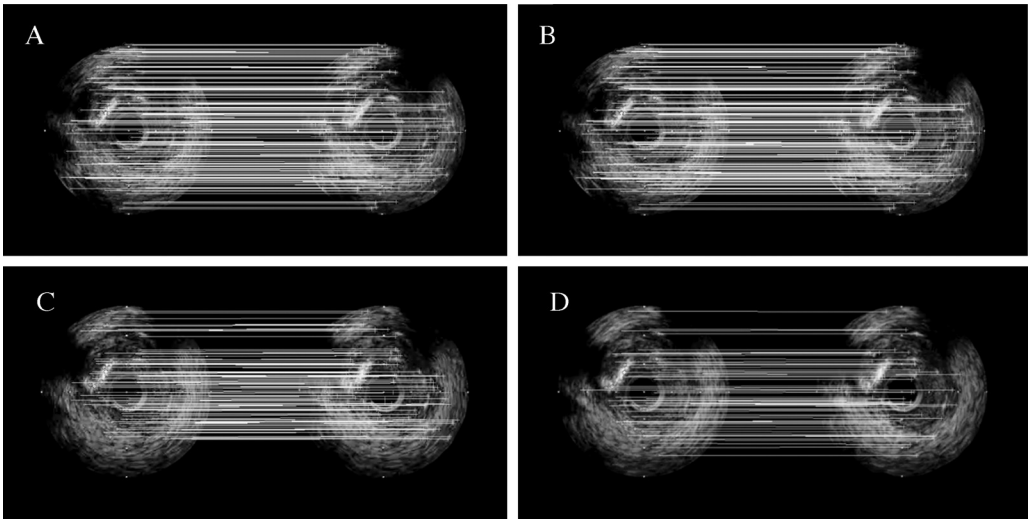

Fig. 5 – Match points (inliers only) for (A) Rigid registration, (B) Affine registration, (C) B-Splines registration, and (D) Demons registration.

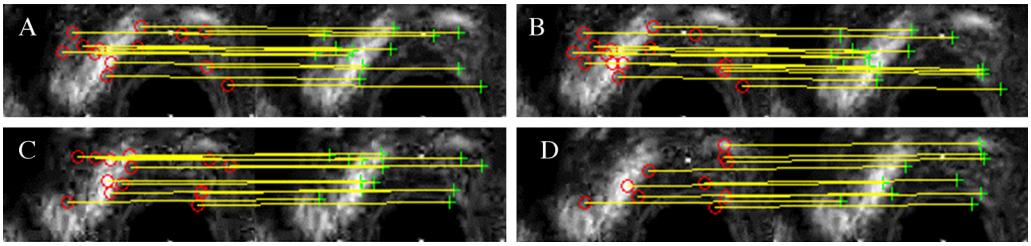

Fig. 6 – ROI match points for (A) Rigid (including outliers), (B) Affine (including outliers), (C) B-Splines (including outliers), and (D) Demons (including outliers).

Please cite this article in press as: T. Araki, et al., A comparative approach of four different image registration techniques for quantitative assessment of coronary artery calcium lesions using intravascular ultrasound, Comput. Methods Programs Biomed. (2014), http://dx.doi.org/10.1016/j.cmpb.2014.11.006

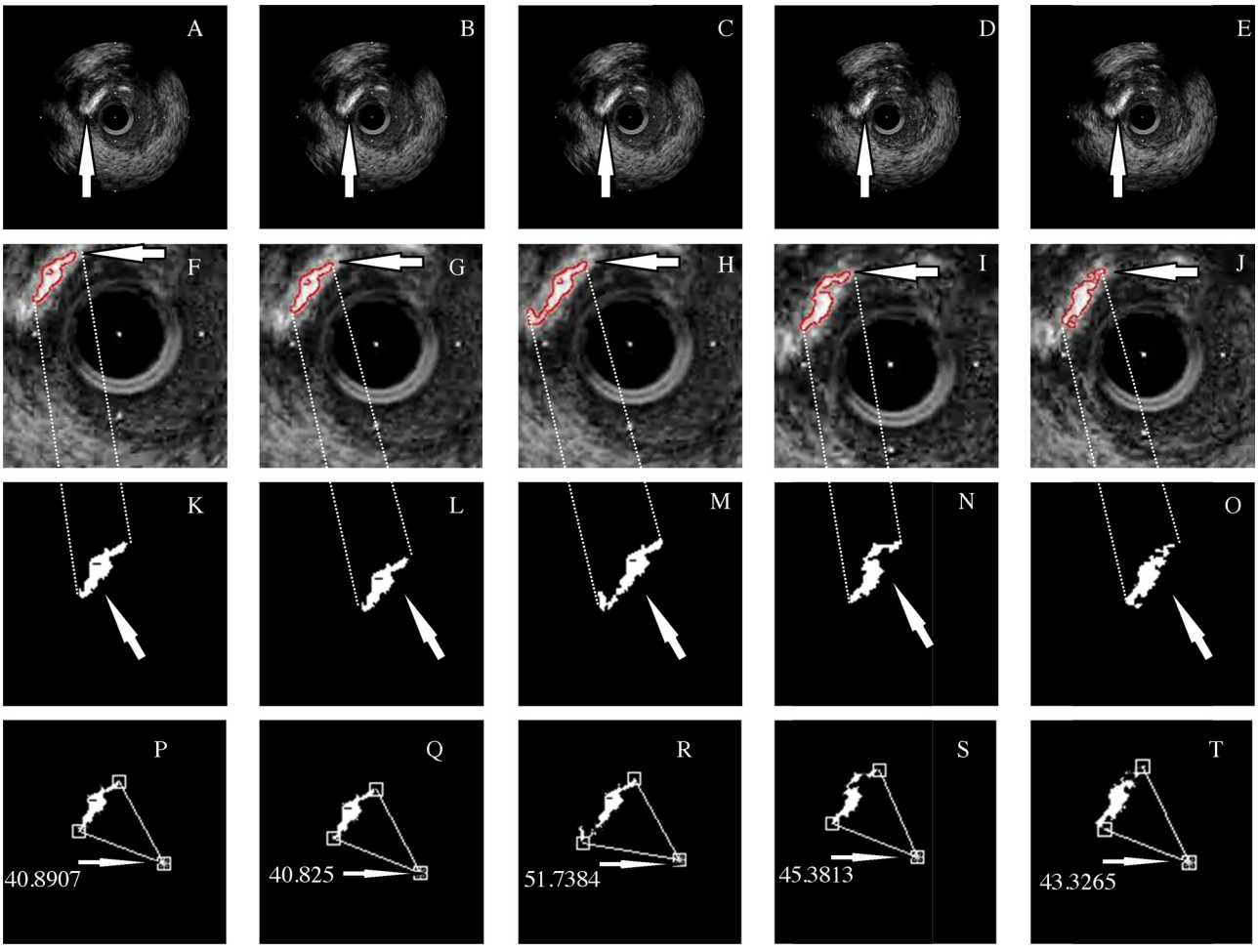

Fig. 7 – Row 1: (A) original calcium detected frame before registration (solid arrow), (B) original calcium detected frame after registration using Rigid (solid arrow), (C) original calcium detected frame after registration using Affine (solid arrow), (D) original calcium detected frame after registration using B-Splines (solid arrow), (E) original calcium detected frame after registration using Demons (solid arrow). Row 2: (F) ROI before registration, (G) ROI after registration using Rigid, (H) ROI after registration using Affine (I) ROI after registration using B-Splines, (J) ROI after registration using Demons. Row 3: (K) detected lesion area before registration (solid arrow), (L) detected lesion area after registration using Demons (solid arrow), (M) detected lesion area after registration using B-Splines (solid arrow), (N) Detected lesion area after registration using B-Splines (solid arrow), (O) detected lesion area after registration using Demons (solid arrow). Row 4: (P) detected lesion arc before registration (solid arrow), (Q) lesion arc after registration using Rigid (solid arrow). (R) Lesion arc after registration (solid arrow) using Affine. (S) Lesion arc after registration using B-Splines (solid arrow). (T) Lesion arc after registration (solid arrow) using Demons.

The polar plot also helps to understand the spatial changes of lesion arc and lesion's distance from catheter centre before and after registration process.

3.5. *ROC analysis: correlation of cIMT with calcium volumes*

Given the evidence that there may be correlation between carotid plaque characteristics such as cIMT (obtained using AtheroEdge^{TM}, AtheroPoint^{TM} LLC, Roseville, California, USA) and coronary plaque calcium burden, we assessed the relationship between cIMT thickness (as a reference standard) and coronary calcium volumes (before and after registration). From the ROC curve analysis, we observed that, by using 1.0 mm as the threshold for cIMT marking higher risk atherosclerotic changes. We observed an improvement of 3.04% in area under curve (AUC) for computed normalized volume using Rigid and Affine. A 2.66% improvement can be seen in AUC for computed normalized volume using B-Splines. We acknowledge that this analysis assumes a high level of correlation between cIMT and coronary calcium as well as choosing a single threshold to define abnormal or high-risk cIMT. These assumptions, including the nature of discordant atherosclerotic disease characteristics in the carotid and coronary vascular beds requires further investigations. It also establishes that future studies should be more characterize. In spite of these issues, IVUS registration clearly improved the correlation between cIMT and coronary plaque calcification

Please cite this article in press as: T. Araki, et al., A comparative approach of four different image registration techniques for quantitative assessment of coronary artery calcium lesions using intravascular ultrasound, Comput. Methods Programs Biomed. (2014), http://dx.doi.org/10.1016/j.cmpb.2014.11.006

Table 1 – Effect of registration on lesion quantification parameters.

Parameters		Rigid registration			Affine registration		B-Splines registration		Demons registration	
Measured variable (Mean)	Before registration	After registration (Rigid)	(%) Difference	After registration (Affine)	(%) Difference	After registration (B-Splines)	(%) Difference	After registration (Demons)	(%) Difference
Lesion length	1.52 ± 0.47 mm	1.44 ± 0.29 mm	5.27	1.42 ± 0.30 mm	6.50	1.39 ± 0.57 mm	8.81	1.40 ± 0.32 mm	7.94
Distance from catheter centre	1.92 ± 0.41 mm	1.83 ± 0.47 mm	4.57	1.81 ± 0.49 mm	5.94	1.77 ± 0.63 mm	7.99	1.75 ± 0.46 mm	8.92
Lesion arc	23.45° ± 8.35°	22.08° ± 6.69°	5.84	21.93° ± 6.57°	6.50	21.57° ± 10.12°	8.67	21.57° ± 6.81°	8.02
Lesion subtended angle	181.18° ± 66.44°	170.51° ± 68.99°	5.88	167.98° ± 68.81°	7.28	163.88° ± 80.65°	9.34	162.86° ± 68.53°	10.11
Lesion area	0.095 ± 0.029 mm^2	0.091 ± 0.018 mm^2	4.92	0.089 ± 0.019 mm^2	6.06	0.088 ± 0.038 mm^2	8.41	0.089 ± 0.021 mm^2	6.75
Lesion normalized volume	0.0019 ± 0.0018 mm^3	0.0018 ± 0.0004 mm^3	5.67	0.0018 ± 0.0004 mm^3	6.66	0.0017 ± 0.0004 mm^3	7.91	0.0017 ± 0.0004 mm^3	7.23

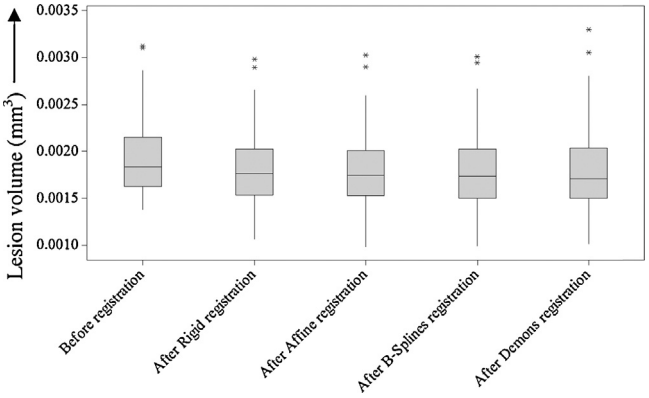

Fig. 8 – Box Plot of calcium lesion volume before and after registration using Rigid, Affine, B-Splines and Demons registration.

based on our definitions. The general analysis of ROC curve is reported in Table 2. The effect of registration on ROC curve is shown in Fig. 10.

4. Performance evaluation

4.1. *Similarity measures of the lesion via overlap ratio*

The overlap ratio (OR′) is calculated to measure the similarity of the binary calcium segmented region before and after registration. The overlap ratio can be expressed as:

$$OR' = \frac{TP'}{TP' + FN' + FP'}$$

where, TP′ refers to true positive, false positive is FP and FN is false negative. Total overlapping lesion area where calcium is detected at the same location before and after registration is known as TP′ or true positive. FN′ is measured by subtracting TP′ (overlapping area) from the total lesion area estimated prior to registration. Similarly, FP′ is computed by subtracting TP′ (overlapping area) from the total lesion area estimated after the registration.

The overlap region of lesion before and after registration using Rigid, Affine, B-Splines, and Demons are illustrated in Fig. 11. Table 3 shows the overlap ratio comparison among the different types of registration methods we studied. Rigid showed a 5.91% difference before and after the registration while Affine registration results showed a percentage difference of 6.23%. Results noted before and after registration using B-Splines and Demons showed lesser percentage differences of 3.05% and 4.48%, respectively.

4.2. *Structural similarity index*

Structural and feature based similarity indices check for the similarity by extracting structural and transformed features from the images. To derive the similarity of structure based features between the reference and target images, structural similarity index (SSIM) and mean structural similarity index (MSSIM) are computed.

Please cite this article in press as: T. Araki, et al., A comparative approach of four different image registration techniques for quantitative assessment of coronary artery calcium lesions using intravascular ultrasound, Comput. Methods Programs Biomed. (2014), http://dx.doi.org/10.1016/j.cmpb.2014.11.006

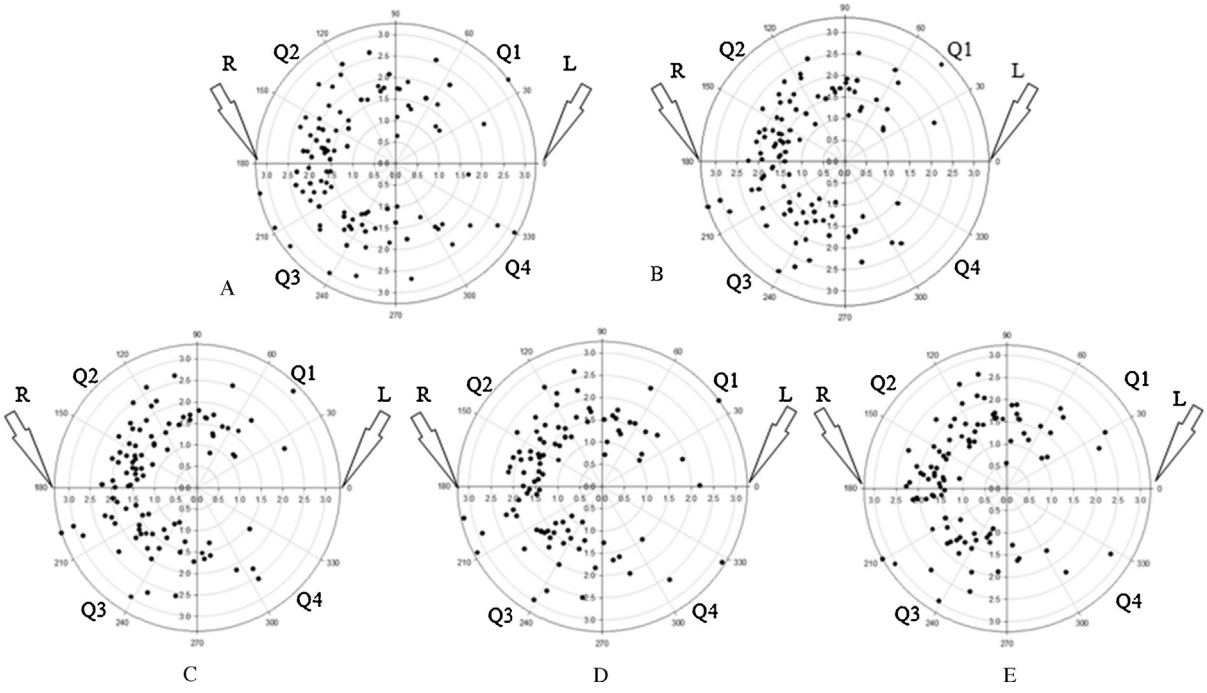

Fig. 9 – Polar plot showing the relative location of calcium lesion along the circumference per volume (A) before registration, (B) after Rigid registration, (C) after Affine registration, (D) B-Splines registration, (E) after Demons registration.

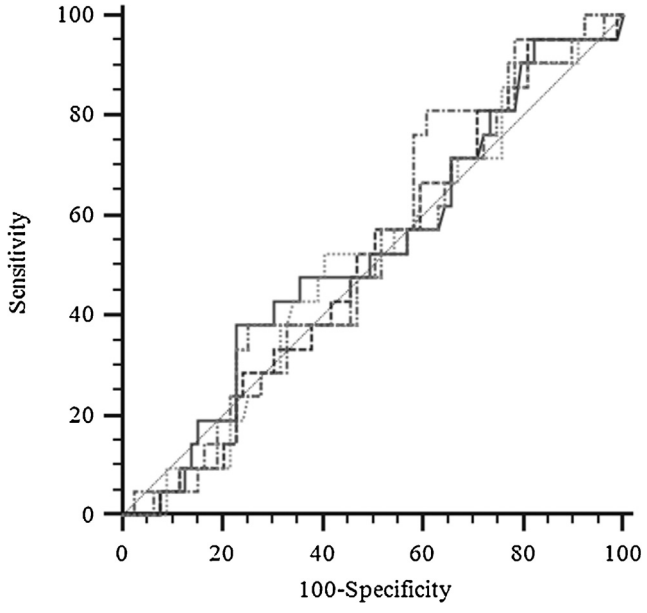

Fig. 10 – ROC curve analysis for cIMT vs. normalized volume (integration method), before registration (solid black), after Rigid registration (dashed double dotted black), after Affine registration (dashed black), after B-Splines registration (dotted black), after Demons registration (dashed dotted black).cIMT, computed by AtheroEdge™, AtheroPoint™ LLC, Roseville, CA, USA.

SSIM and MSSIM are defined as:

$$\mathrm{SSIM} = \frac{(2\upsilon_x\upsilon_y + k_1)(2a_{xy} + k_2)}{(\upsilon_x^2 + \upsilon_y^2 + k_1)(a_x^2 + a_y^2 + k_2)} \quad (5)$$

where, x is the reference (before registration) image, y is the query (after registration) image, υ_x is the average of the reference image (x), υ_y is the average of the query image (y), α_x is the standard deviation of reference image (x), α_y is the standard deviation of query image (y), υ_{xy} is the covariance of x and y, k_1 and k_2 are variable to stabilize the division with weak denominator. MSSIM is given by Choi and Lee [26]

$$\mathrm{MSSIM}(x, y) = \frac{1}{N}\sum_{i=1}^{N}\mathrm{SSIM}(x_i - y_i) \quad (6)$$

where, N is the number of local windows in an image. The structural coefficients and overlap measures vary between zero and one. The ideal value is one and that represents prefect overlap in the images. Table 3 reports the overlapping percentage of binary calcium lesion as an effect of registration (Rigid, Affine, Demons and B-Splines) and it also reports the mean structural similarity index (MSSIM) between original grey frames and registered grey frames of all 100 patients (Fig. 12).

5. Discussion

The objective of our current study was to: (i) obtain correct shape-based lesion quantification parameters and (ii) analysis of shape and size change of detected calcium in culprit IVUS frames to study the effect of registration. To accomplish these objectives, we compared and contrasted four different IVUS registration techniques: (a) Rigid, (b) Affine, (c) B-Splines, and (d) Demons registration.

Please cite this article in press as: T. Araki, et al., A comparative approach of four different image registration techniques for quantitative assessment of coronary artery calcium lesions using intravascular ultrasound, Comput. Methods Programs Biomed. (2014), http://dx.doi.org/10.1016/j.cmpb.2014.11.006

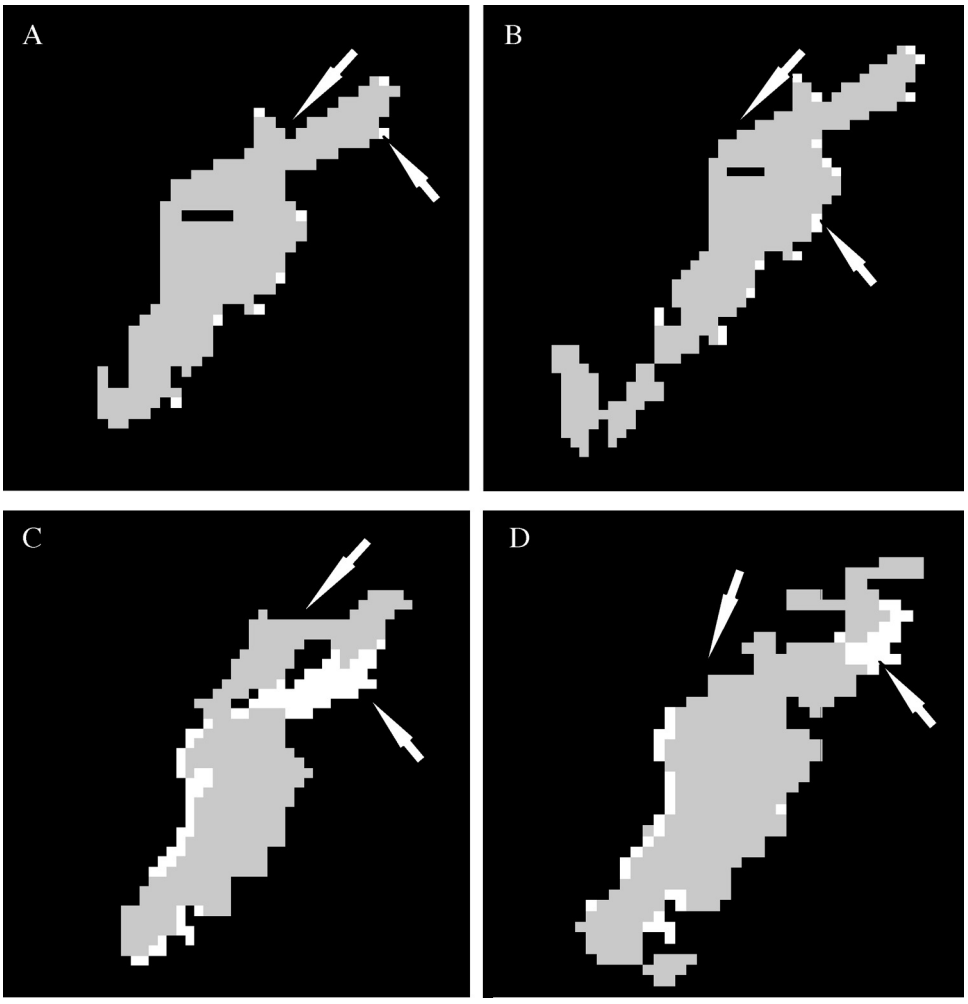

Fig. 11 – (A) Lesion overlapping – before registration (*up arrow*) and after Rigid registration (*down arrow*), (B) Lesion overlapping – before registration (*up arrow*) and after Affine registration (*down arrow*), (C) Lesion overlapping – before registration (*up arrow*) and after B-Splines registration (*down arrow*), (D) Lesion overlapping – before registration (*up arrow*) and after Demons (*down arrow*).

Rigid and Affine registration are more focussed on the simple steps of transformations like rotation or scaling. Non-rigid B-Splines registration is a type of deformable image registration (DIR) process. DIR leads to accurate quantification, by mapping the functional, spatial, anatomical, and biological variations for different images. B-Splines FFD is mainly adapted by maximizing the similarity measure between different images. Demons algorithm is completely local transformation model unlike B-Splines, which offers semi-local transformations.

In this current study we have considered the following quantification parameters: (i) the mean lesion length, (ii) mean lesion distance from catheter, (iii) mean lesion arc, (iv) mean lesion span, (v) mean lesion area, and (vi) normalized volume. The results of these lesion quantification parameters, before and after registration are shown in Table 1. As seen in this

Table 2 – ROC curve for cIMT vs. calcium volume.

	Before registration	After Rigid registration	After Affine registration	After B-Splines registration	After Demons registration
Variable: calcium volume (IM) and classification variable: cIMT					
Total no. of volume	100 (cIMT value was NAN for 7 cases)				
Positive group: IMT = 1.0	14	14	14	14	14
Negative group: IMT = 1.0	79	79	79	79	79
Area under the ROC curve (AUC)	0.527	0.511	0.511	0.513	0.527
Standard error	0.0708	0.0697	0.0672	0.0684	0.0653
95% Confidence interval	0.388–0.666	0.375–0.648	0.379–0.643	0.379–0.647	0.399–0.655

Please cite this article in press as: T. Araki, et al., A comparative approach of four different image registration techniques for quantitative assessment of coronary artery calcium lesions using intravascular ultrasound, Comput. Methods Programs Biomed. (2014), http://dx.doi.org/10.1016/j.cmpb.2014.11.006

Table 3 – Similarity measures of lesion.

Measured variable (mean)	Before registration	After registration (Rigid)	(%) Difference	After registration (Affine)	(%) Difference	After registration (B-Splines)	(%) Difference	After registration (Demons)	(%) Difference
Overlapping	50.3542 ± 14.2349	47.3779 ± 14.0849	5.91	47.2188 ± 14.2079	6.23	51.8931 ± 14.2901	3.05	48.0971 ± 14.9457	4.48
MSSIM		0.9987 ± 0.00069		0.9986 ± 0.00073		0.9979 ± 0.00082		0.9984 ± 0.00073	

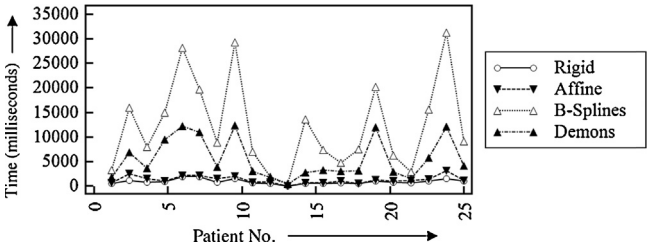

Fig. 12 – Time comparison between different types of registration (25 patients sample).

table, there is a reduction of these quantification parameters in all the four registration methods. We further observed that the percentage difference of these quantification parameters before and after the registration was highest to lowest in the following order: B-Splines, Demons, Affine, and Rigid. This signifies B-Splines have the largest ability to capture the change during the registration process. Even though, B-Splines offer certain advantages in terms of statistical accuracy, it is proved to be one of the slowest when it comes to time complexity. In Table 4, we demonstrated the time comparison between four different types of registration. The time taken for registration per frame was largest for B-Splines (105.38 s) compared to low time complexity of Rigid (8.37 s), Affine (10.93 s) and Demons (49.95 s). The main attribute of Rigid and Affine is its simplicity, smoothness and least amount of processing steps needed during the registration process. This accounts the fastest speed for Rigid and Affine.

Table 5, represents the parameters adapted in these four registration techniques, namely, Rigid, Affine, B-Splines and Demons. The table is divided the tables into four divisions (a)–(d) corresponding to the four techniques. Table 5(a) depicts the five different kinds of parameters, which is helpful in optimization of the Rigid and Affine registration methods. They are Gradient Magnitude Tolerance, Minimum Step Length, Maximum Step Length, Maximum Iterations, and Relaxation Factor. The default values can be seen in the table. Similarly, the parameters adapted by Affine, B-Splines and Demons registration can be seen in the corresponding Table 5(b)–(d). These parameters are responsible for the sensitivity in registration processes. For example, during the Affine registration processes, number of histogram bins [4], and use all pixels [7] and number of spatial samples are more sensitive compared to the other parameters. To control the optimization process in Rigid and Affine registration, Gradient Magnitude Tolerance is used. It is a positive scalar value. When the value of the gradient is smaller than Gradient Magnitude Tolerance, it means that the optimizer might have reached a plateau. The default value of Gradient Magnitude Tolerance is 10^{-4} mm^{-1}. To control the accuracy of convergence Minimum Step Length is used. It is also a positive scalar value. If Minimum Step Length is set to a small value, the optimization takes longer to compute, but it is likely to converge on a more accurate metric value. The default value of Minimum Step Length is 1.5×10^{-5} mm. Maximum Step Length controls the initial step length used in optimization. If the Maximum Step Length is set to a larger value, the computation time decreases. However, the optimizer might fail to converge if Maximum Step Length is set

Please cite this article in press as: T. Araki, et al., A comparative approach of four different image registration techniques for quantitative assessment of coronary artery calcium lesions using intravascular ultrasound, Comput. Methods Programs Biomed. (2014), http://dx.doi.org/10.1016/j.cmpb.2014.11.006

Table 4 – Time comparison between different types of registration.

Registration types	Rigid	Affine	B-Splines	Demons
Mean time/frame	0.321357892	0.419619303	4.043311874	1.916635413
Mean time/reg. frame	8.375594733	10.93659532	105.3813908	49.95353113

to an overly large value. The default value of Maximum Step Length is 0.0625 mm. Relaxation Factor is an internal debugging parameter [8] having scalar value between 0 and 1. It defines the rate at which the optimizer reduces step size during convergence. The parameters adapted in B-Splines are grid dimension, number of grid refinements, and total number of iterations (see Table 5(c)). Since the grid dimensions are $4 \times 4\,\text{pixel}^2$, which implies the grid is refined four times during the registration process. If the numbers of iterations are kept to a fixed value of 10, then B-Splines are leading to a better convergence compromising the time complexity. On the contrary, Demons adapts to three set of parameters (see Table 5(d)) which are helpful to improve the performance in terms of accuracy and speed.

Another feature which our system offers is the ability to show the global representation and layout of the calcium lesions in polar form. This polar representation shows dotted points which corresponds to the centre of the calcium lesions. Fig. 9 shows the location of calcium lesion along the circumference per volume corresponding to these four different registration methods. As can be seen in the polar representation, the mean distance of the lesions from the catheter centre is highest for Rigid (1.83 mm) and comparable to Affine (1.81 mm), while lower in B-Splines (1.77 mm) and comparable to Demons (1.75 mm). Though the plots are suppose to signify the cohort's behaviour of calcium lesions along the circumventer, our observations only show that most of calcium lesions are in sector Q2 followed by Q3.

As part of the data analysis and performance, we evaluated the overlapping regions. We showed in Fig. 11 and Table 3 that B-Splines and Demons showed a lower percentage differences compared to Rigid and Affine, which came to be higher than B-Splines and Demons. We also showed the feature point matching technique between the reference and target frames. As shown in Figs. 4–6 are the strongest feature points are same before and after the registration. As part of the performance, we observed the ROC curve between cIMT and calcium volume, before and after the registration. Table 2 reports the area under ROC curve which is highest for Demons ($0.527\,\text{mm}^2$) when compared against Rigid ($0.511\,\text{mm}^2$), Affine ($0.511\,\text{mm}^2$) and B-Splines ($0.513\,\text{mm}^2$) registration techniques. Further, Table 2 also shows that the Rigid (0.0697) and Affine registration (0.672) techniques having higher standard error compared to B-Splines (0.0684) and Demons (0.0653) techniques, respectively.

Apart from comparing different registration techniques and lesion quantification parameters, our proposed system was also focussed on the intermediate stage of calcium segmentation during volume computation. As previously noted, we converted the IVUS videos to QuickTime (.mov) file extension, for our study. Each IVUS video were broken into multiple IVUS frames, with each frame (or image)'s resolution being

Table 5 – Registration parameters: Rigid, Affine, B-Splines and Demons.

Total no. of volume			100
Mean no. of registered frames/volume			95
Window size in MSSIM			$8 \times 8\,\text{pixels}^2$
Bin size			10
(a) Common registration parameters in Rigid and Affine registration			
Optimizer	Gradient Magnitude Tolerance		10^{-4} (mm^{-1})
	Minimum Step Length		1.5×10^{-5} (mm)
	Maximum Step Length		6.25×10^{-2} (mm)
	Maximum Iterations		1000
	Relaxation Factor		5×10^{-1}
(b) Extra registration parameters in Affine registration			
Metric	Number of spatial samples		500
	Number of histogram bins		50
	Use all pixels		True
(c) Registration parameters in B-Splines registration			
Grid dimension			$4 \times 4\,\text{pixels}^2$
Number of grid refinements			4
Total number of iterations			10
(d) Registration parameters in Demons registration			
Total number of iterations		200	
Velocity field smoothing kernel	2-D filter		Sigma
	Gaussian low pass filter		10 pixels
Alpha (noise) constant		2.5 dB	

Please cite this article in press as: T. Araki, et al., A comparative approach of four different image registration techniques for quantitative assessment of coronary artery calcium lesions using intravascular ultrasound, Comput. Methods Programs Biomed. (2014), http://dx.doi.org/10.1016/j.cmpb.2014.11.006

512×512. To observe the lesion changes before and after image registration (using different techniques) we needed to extract the lesion from the IVUS frames. In order to do that, our proposed system went through few steps. We first set up a binning strategy, which would help to solve the problem caused by spatio-temporal localization changes of lesion. This step was used until the total video containing all bins were processed. To improve the image quality and adventitia mask generation, median filtering was used. We also used Otsu's local statistical threshold method to binarize the generated image. Connected component analysis (CCA) was used to remove scattered binary lumen regions from the binary image as well as it to obtain maximum binary adventitia. Finally, Otsu's local statistical threshold method helped to extract the only bright region of calcium. Retaining the white dotted markers in IVUS frames the calcium region was segmented. From extracted lesion we managed to calculate the overlapped changes before and after registration (Table 3). This table reports, the overlapping changes in lesion are minimal during B-Splines and Demons registration. Affine registration led to the highest change in overlap of lesion, followed by rigid registration. As previously noted, this comparison also helped to establish the B-Splines method is more optimal compared to other three methods with Rigid and Affine registration being the worse selection among all.

Compared to previous IVUS registration methods introduced by Veress et al. [7], Rotger et al. [8], Amores and Radeva [13] and Oakeson et al. [14], our method not only focussed on the segmentation part, but also on the changes of IVUS detected coronary lesion's shape and quantification before and after the registration. As atherosclerotic calcium deposits are multifocal in nature, there is always a chance of under-estimation of calcium volume computation [5,6] using our proposed segmentation technique. The main objective of this research was to increase the correlation between two consecutive frames for improved spatio-temporal localization of coronary calcium plaque. Towards this end, we focused primarily on IVUS registration rather than segmentation unlike some previous works. Compared to previews IVUS image registration analysis and review studies, proposed by Pluim et al. [29], Liang et al. [30], Guo et al. [31], Makni et al. [32], Khalifa et al. [33] and Oliveira and Tavares [34] our proposed technique was quite unique, as it established a comparative study between four different registration techniques. Using the lesion quantification parameters table, comparison of visual representation of lesion changes before and after registration, calcium detection and volume computation prior to registration, the box plot of lesion volume, the polar representation of the quantification parameters, ROC curve analysis, similarity structure measure of lesion overlap after registration and finally the processing time comparison of different registration techniques, we managed to successfully establish the comparative study among all four registration technique. Calcium segmentation and detection from low contrast video are out of the scope of the current research. This study remains pilot in nature and requires further validation using CTA. Future work may consist of adapting these registration methods on large cohorts. Further looking into different components of plaque compared to just calcium and utilize that for registration.

6. Conclusion

Our main focus in this study was to compare different registration techniques and their effect on calcium quantification and detection via IVUS. Such applications are an assistive tool in planning coronary endarterectomy procedures or during coronary stenting procedures, which are direct clinical translations of our work. In order to compare different registration techniques, we used some lesion quantification parameters and their results before and after registration. This study aids in the accurate quantification of calcium in coronary plaque and also compares the effect of a parametric and a non-parametric registration method on IVUS imaging. Optimizing IVUS imaging registration methods for calcium detection requires consideration of the tradeoffs that are inherent between speed, accuracy, robustness, and smoothness of the registration transformation. Such an approach is a more realistic assessment of the relative merits of each registration method rather than categorically stating that any one single method is superior in all situations. With the promising results from this study, it can be assumed that larger scale prospective studies need to be tried for computing calcium volume post-registration and correlated to carotid IMT and corroborated against CTA.

REFERENCES

[1] P. Libby, P.M. Ridker, G.K. Hansson, Progress and challenges in translating the biology of atherosclerosis, Nature 473 (2011) 317–325.
[2] Y. Honda, T. Toyama, Y. Miyaishi, H. Kan, R. Kawaguchi, H. Adachi, H. Hoshizaki, S. Oshima, Coronary artery calcification as a new predictor of non-target lesion revascularization during the chronic phase after successful percutaneous coronary intervention, Cardiovasc. Interv. Ther. (2014).
[3] M.A. de Graaf, A. Broersen, P.H. Kitslaar, C.J. Roos, J. Dijkstra, B.P. Lelieveldt, J.W. Jukema, M.J. Schalij, V. Delgado, J.J. Bax, J.H. Reiber, A.J. Scholte, Automatic quantification and characterization of coronary atherosclerosis with computed tomography coronary angiography: cross-correlation with intravascular ultrasound virtual histology, Int. J. Cardiovasc. Imaging 29 (5) (2013) 1177–1190.
[4] A. Arbab-Zadeh, A.N. DeMaria, W.F. Penny, R.J. Russo, B.J. Kimura, V. Bhargava, Axial movement of the intravascular ultrasound probe during the cardiac cycle: implication for three-dimensional reconstruction and measurements of coronary dimensions, Am. Heart J. 138 (1999) 865–872.
[5] T. Araki, N. Ikeda, F. Molinari, N. Dey, S. Acharjee, L. Saba, A. Nicolaides, J.S. Suri, Effect of geometric-based coronary calcium volume as a feature along with its shape-based attributes for cardiological risk prediction from low contrast IVUS, J. Med. Imaging Health Inform. 4 (2014) 255–261.
[6] T. Araki, N. Ikeda, F. Molinari, N. Dey, S. Acharjee, L. Saba, J.S. Suri, Link between automated coronary calcium volumes from intravascular ultrasound (IVUS) to automated carotid IMT from B-mode ultrasound in coronary artery disease population, Int. Angiol. 33 (4) (2014) 392–403.
[7] I. Veress, J.A. Weiss, T. Grant, D.G. Gullberg, R.D. Vince, Rabbitt, Strain measurement in coronary arteries using intravascular ultrasound and deformable images, J. Biomech. Eng. 124 (2002) 734–741.

Please cite this article in press as: T. Araki, et al., A comparative approach of four different image registration techniques for quantitative assessment of coronary artery calcium lesions using intravascular ultrasound, Comput. Methods Programs Biomed. (2014), http://dx.doi.org/10.1016/j.cmpb.2014.11.006

[8] D. Rotger, P. Radeva, E. Fernández-Nofrerías, J. Mauri, Multimodal registration of intravascular ultrasound images and angiography, in: Proceedings of the XX Congreso Anual de la Sociedad Espanola de Ingenieria Biomedica (CASEIB), 2002, pp. 137–140.
[9] A. Katouzian, A. Karamalis, D. Sheet, E. Konofagou, B. Baseri, S.G. Carlier, A. Eslami, A. König, N. Navab, A.F. Laine, Iterative self-organizing atherosclerotic tissue labeling in intravascular ultrasound images and comparison with virtual histology, IEEE Trans. Biomed. Eng. 59 (11) (2012) 3039–3049.
[10] J.B. Lindsey, J.A. House, K.F. Kennedy, S.P. Marso, Diabetes duration is associated with increased thin-cap fibroatheroma detected by intravascular ultrasound with virtual histology, Circ. Cardiovasc. Interv. 2 (6) (2009) 543–548.
[11] C.P. Loizoua, C. Theofanousb, M. Pantziarisc, T. Kasparisb, Despeckle filtering software toolbox for ultrasound imaging of the common carotid artery, Comput. Methods Programs Biomed. 114 (1) (2014) 109–124.
[12] T.-H. Wua, C.-J. Linb, Y.-H. Lina, W.-Y. Guob, T.-C. Huangd, Quantitative analysis of digital subtraction angiography using optical flow method on occlusive cerebrovascular disease, Comput. Methods Programs Biomed. 111 (3) (2013) 693–700.
[13] J. Amores, P. Radeva, Non-rigid registration of vessel structures in IVUS images Pattern Recognition and Image Analysis, vol. 2652, Springer-Verlag, 2003, pp. 45–52.
[14] K.D. Oakeson, H. Zhu, Morton, Quantification of cross-sectional artery wall motion with IVUS image registration, Proc. Int. Soc. Opt. Photon. 1 (2004) 119–130.
[15] C. Gatta, O. Pujol, O. Rodriguez-Leor, J. Mauri, P. Radeva, Fast rigid registration of vascular structures in IVUS sequences, IEEE Trans. Inf. Technol. Biomed. 13 (6) (2009) 1006–1011.
[16] S. Balocco, C. Gatta, F. Ciompi, O. Pujol, X. Carrillo, J. Mauri, P. Radeva, Combining growcut and temporal correlation for IVUS lumen segmentation Pattern Recognition and Image Analysis, vol. 6669, 2011, pp. 556–563.
[17] A. Gupta, H.K. Verma, S. Gupta, A hybrid framework for registration of carotid ultrasound images combining iconic and geometric features, Med. Biol. Eng. Comput. 51 (2013) 1043–1050.
[18] H. Rivaz, Z. Karimaghaloo, D.L. Collins, Self-similarity weighted mutual information: a new non-rigid image registration metric, Med. Image Anal. 18 (2014) 343–358.
[19] P. Wang, O. Ecabert, T. Chen, M. Wels, Image-based co-registration of angiography and intravascular ultrasound images, IEEE Trans. Med. Imaging 32 (2013) 2238–2249.
[20] S. Gu, X. Meng, F.C. Sciurba, H. Ma, J. Leader, N. Kaminski, D. Gur, J. Pu, Bidirectional elastic image registration using B-Splines Affine transformation, Comput. Med. Imaging Graph. (2014).
[21] E.R. Denton, L.I. Sonoda, D. Rueckert, S.C. Rankin, C. Hayes, M.O. Leach, D.L. Hill, D.J. Hawkes, Comparison and evaluation of rigid, affine, and non-rigid registration of breast MR images, J. Comput. Assist. Tomogr. 5 (1999) 800–805.
[22] H.M. Garcia-Garcia, M.A. Costa, P.W. Serruys, Imaging of coronary arthrosclerosis: intravascular ultrasound, Eur. Heart J. 3 (2010) 2456–2469.
[23] N. Otsu, A threshold selection method from gray-level histograms, IEEE Trans. Syst. Man Cybern. 9 (1) (1979) 62–66.
[24] D. Hanb, N.-T. Doana, H. Shimb, B. Jeonb, H. Leec, Y. Hongb, H.-J. Changb, A fast seed detection using local geometrical feature for automatic tracking of coronary arteries in CTA, Comput. Methods Programs Biomed. 117 (2) (2014) 179–188.
[25] K. Branson, A practical review of uniform B-Splines, 2004.
[26] Y. Choi, S. Lee, Injectivity conditions of 2D and 3D uniform cubic B-Splines functions, Graph. Models 62 (6) (2000) 411–427.
[27] L. Schwarz, Non-rigid registration using free-form deformations (Ph.D. dissertation), Dept. Comput. Sci., Tech. Univ. Munchen, 2007, pp. 27–41.
[28] J.P. Thirion, Image matching as a diffusion process: an analogy with Maxwell's Demons, Med. Image Anal. 2 (1998) 243–260.
[29] J.P.W. Pluim, J.B. Antoine Maintz, M.A. Viergever, Mutual information based registration of medical images: a survey, IEEE Trans. Med. Imaging 22 (2003) 986–1004.
[30] Y. Liang, K.D. Oakeson, H. Zhu, M.H. Friedman, Estimation of arterial wall strain based on IVUS image registration Annual International Conference of the IEEE Engineering in Medicine and Biology Society, vol. 1, 2006, pp. 3218–3221.
[31] Y. Guo, R. Sivaramakrishna, C.C. Lu, J.S. Suri, S. Laxminarayan, Breast image registration techniques, Med. Biol. Eng. Comput. 44 (2006) 15–26.
[32] N. Makni, P. Puech, P. Colin, A. Azzouzi, S. Mordon, N. Betrouni, Elastic image registration for guiding focal laser ablation of prostate cancer, Comput. Methods Programs Biomed. 108 (2012) 213–223.
[33] F. Khalifa, G.M. Beache, G. Gimel'farb, J.S. Suri, A.S. El-Baz, State-of-the-art medical image registration methodologies: a survey Multi Modality State-of-the-Art Medical Image Segmentation and Registration Methodologies, vol. 1, 2011, pp. 235–280.
[34] F.P. Oliveira, J.M. Tavares, Medical image registration: a review, Comput. Methods Biomech. Biomed. Eng. 17 (2) (2014) 73–93.

WEB REFERENCES

[1] http://www.creatis.insa-lyon.fr/~srit/tete/2012_master_eeap_si_m5.pdf (accessed 23.04.14).
[2] http://www.mathworks.in/help/images/ref/registration.optimizer.regularstepgradientdescent-class.html (accessed 23.04.14).
[3] http://www2.cs.uregina.ca/~anima/408/Notes/Interpolation/UniformBSpline.htm (accessed 23.04.14).
[4] https://www.slicer.org/slicerWiki/index.php/Documentation/4.3/Modules/AffineRegistration (accessed 23.04.14).
[5] http://www.mathworks.in/help/images/ref/registration.metric.mattesmutualinformation-class.html (accessed 23.04.14).
[6] https://www.slicer.org/slicerWiki/index.php/Documentation/Nightly/Modules/BRAINSFit (accessed 23.04.14).

Please cite this article in press as: T. Araki, et al., A comparative approach of four different image registration techniques for quantitative assessment of coronary artery calcium lesions using intravascular ultrasound, Comput. Methods Programs Biomed. (2014), http://dx.doi.org/10.1016/j.cmpb.2014.11.006